

Oscillation modes of ultralight BEC dark matter cores

F. S. Guzmán

*Laboratorio de Inteligencia Artificial y Supercómputo, Instituto de Física y Matemáticas,
Universidad Michoacana de San Nicolás de Hidalgo. Edificio C-3,
Cd. Universitaria, 58040 Morelia, Michoacán, México.*

(Dated: December 15, 2024)

Structure formation simulations of ultralight bosonic dark matter, ruled by the Gross-Pitaevskii-Poisson (GPP) system of equations, show that dark matter clumps to form structures with density profiles consisting of a core surrounded by a power-law distribution. The core has a density profile similar to that of spherically symmetric equilibrium configurations of the GPP system. These configurations have been shown to be stable under a variety of perturbations and to have attractor properties. It is interesting to know the dominant frequencies of oscillation of these configurations. One reason is that in formed galaxies the effects of perturbations can trigger observable effects for specific frequency modes. Another reason is that during the process of structure formation, the oscillation modes can help to characterize a core. In this manuscript we present a systematic numerical analysis of the reaction of equilibrium configurations to various axi-symmetric perturbations with modes $l = 0, 1, 2$, $m = 0$. We then calculate the first few oscillation frequencies of equilibrium configurations for each mode.

PACS numbers: keywords: dark matter – Bose condensates

Ultralight spin-less dark matter is one of the dark matter candidates that shows properties that suit the current observational restrictions. Among the convenient properties of this particle are that it is ultralight, with mass of order $m \sim 10^{-22} eV$ [1–3], which implies it has a de Broglie wave-length that can prevent structures to develop cusps at the center of structures, which may be a solution of the cusp core problem [4–8]. At larger scales, there are now structure formation simulations showing that this candidate behaves just like CDM [9, 10]. Another problem possibly addressed by this candidate is the abundance of substructure [1–3, 5, 11]. Another appealing property is that a boson with such a small mass, the critical temperature for Bose-Einstein condensation is $T_c \sim 1/m^{5/3}$ in the TeV scale, which guarantees the condensation could have happened at very early stages [12].

At local scales though, there are interesting problems remaining, for instance the relaxation processes of structures that can involve the gravitational cooling process [13, 14], dynamical friction [15] or appropriate damping terms [16]. Nevertheless, structure formation simulations agree in that ultralight bosonic matter clumps into structures with universal profiles composed of a core, sometimes called solitonic profile, and a surrounding cloud of dark matter that approaches a NFW profile [9, 10, 15, 17, 18].

Various oscillations of cored structures have been found to be interesting and potentially important, for instance in [19] the effects on star clusters is estimated for already formed cores, and in [20] the configuration resulting from head-on mergers shows oscillations with a central density varying in orders of magnitude, which eventually could affect the viability of luminous structures living inside such dynamical environment. For instance, in [21] it was shown that luminous matter, modeled as an n-body

system within the gravitational potential of the condensate after a merger, might not survive such violent processes of relaxation and would be spelled out due to violent oscillations of the final configuration. In a less cataclysmic scenario, during the structure formation process, a core is constantly being perturbed by structures moving around it [15]. If some of the oscillations can represent a warning for the model to be viable or provide the fingerprints of cores, it is important to analyze how the later respond to different types of perturbations. Oscillations in a way, may impose important restrictions or confirm the viability of the model, which is a strong a motivation to present a systematic analysis of the response of cores to perturbations in order to know the essential response modes that can eventually be identified with observations or predictions.

For this analysis we have two basic assumptions, the first one is that the dynamics of ultralight BEC dark matter structures is ruled by the GPP system of equations, which is the combination of the Gross-Pitaevskii equation for the condensate [22], and Poisson's equation sourced by the density of the condensate itself, whose solution provides the potential trap that contains the condensate bounded in a region. The second assumption is that cores are spherically symmetric equilibrium configurations of the GPP system [14, 23] as commonly assumed [9, 10, 15, 17].

Additional information is, that one can take a perturbative approach since it is well known these equilibrium configurations are stable under a variety of spherical and axial perturbations, and also show a late-time attractor behavior, which means that eventually fluctuations with an arbitrary initial profile would tend toward one of these equilibrium configurations [13, 14, 24]. Therefore, the method used here to study the modes triggered by various perturbations, consists in the application of per-

turbations to equilibrium configurations, solve the full GPP system of equations in time and diagnose the evolution of physical quantities of the system. In order to be concise, in this paper we concentrate the analysis to axially symmetric perturbations only, which provide the fundamental oscillation modes.

The GPP system of equations in variables absorbing the constants \hbar , G , the boson mass m and the s -wave scattering length among bosons is

$$\begin{aligned} i\frac{\partial\Psi}{\partial t} &= -\frac{1}{2}\nabla^2\Psi + V\Psi + \Lambda|\Psi|^2\Psi \\ \nabla^2 V &= 4\pi|\Psi|^2 \end{aligned} \quad (1)$$

where $\Psi = \Psi(t, \mathbf{x})$ is the parameter order describing the macroscopic behavior of the boson gas, $\rho = |\Psi|^2$ is de gas density, Λ is the self-interaction coefficient, and the potential $V = V(t, \mathbf{x})$ is the gravitational potential sourced by the gas density itself, which in general can depend on time if $|\Psi|^2$ does. Here, as in most of the recent analysis of structure formation and interaction between structures, we assume $\Lambda = 0$, which is the free field case commonly named the fuzzy dark matter regime [25].

The equilibrium configuration that we are to perturb. These configurations are constructed assuming a harmonic time dependence of the wave function $\Psi_e = e^{-i\gamma t}\psi(\mathbf{x})$ and spherical symmetry $\psi = \psi(r)$. In this case the equations above reduce to a stationary system because $|\Psi|^2$ is time-independent, which implies $V = V(r)$ is also-time independent and Schroedinger's equation can be cast as a stationary equation with solution $\psi = \psi(r)$. The resulting equations are solved in the domain $r = [0, r_{max}]$ as a Sturm-Liouville problem for the eigenvalue γ as described in [23], provided boundary conditions of regularity at the origin for $\psi(r)$ and $V(r)$, and isolation conditions at the outer boundary, namely a monopolar potential satisfying $-M/r_{max}$ and ψ and its radial derivative should vanish within a given tolerance at the outer boundary.

The solution defines a one-parameter family of solutions that relates the central value of the wave function $\psi(0)$ and the eigenfrequency γ . Due to the known scale transform that leaves system (1) invariant, $\{t, x, \psi\} \rightarrow \{\hat{t}/\lambda^2, \hat{x}/\lambda, \lambda^2\hat{\psi}\}$ for an arbitrary value of λ , it is enough to solve for one central value $\psi(0)$ and the whole family for all other possible values of this central value will be automatically found. The workhorse configuration corresponds to the case $\psi(0) = 1$, which in turn implies the central density is also one, has an eigenvalue $\gamma = 0.69223$, mass $M = 2.0622$ and $r_{95} = 3.93$ [23], numbers that will be helpful later on. The scale invariance allows one to study the properties, evolution, and -for the purpose of this paper- the reaction to perturbations of only this workhorse configuration, and the results can be rescaled to all the other possible configurations. This is the reason why we will perturb this particular case in the reminder of the manuscript.

Perturbations. The perturbation applied to the wave function of the equilibrium configuration is a spherical shell with thickness σ_p , centered at a distance r_p from the center of the configuration itself, launched with radial wave number k_r and shape proportional to specific spherical harmonics. Since we only consider axially symmetric perturbations, we will only involve modes (l, m) with $l = 0, 1, 2$ and $m = 0$, The expression used for the perturbation is

$$\begin{aligned} \Psi_0 &= \Psi_e + \delta\Psi, \\ \delta\Psi &= e^{-ik_r\sqrt{\varrho^2+z^2}} a_{l0} Y_l^0, \\ a_{l0} &= A_{l0} e^{-(\sqrt{\varrho^2+z^2}-r_p)^2/\sigma_p^2}. \end{aligned} \quad (2)$$

where Ψ_e is the wave function of the equilibrium configuration. In order to have a consistent gravitational potential, one solves Poisson equation sourced by the density $|\Psi_0|^2$ at initial time. Then we track the evolution of the perturbed system by numerically solving (1) and analyze its behavior.

We use perturbations proportional to each mode (l, m) separately in order to study their impact on the oscillations of the configuration. In all the cases we set $r_p = 2r_{95}$ and the thickness of the shell to $\sigma_p = 1$. In order to make sure the modes triggered by the perturbation are wave-number independent we use three values $k_r = 0, 1, 2$. The amplitudes A_{l0} are fine-tuned in such a way that the initial total mass of the perturbed configuration is $M = M_e + \delta M$, where $M_e = 2.0622$ is the mass of the equilibrium configuration in standard code units (as in [23]) and the perturbation mass is $\delta M = 0.1\%$ and 0.5% of M_e . Then for each value of k_r and δM such fine-tuning is required.

Spherically symmetric evolution for spherical modes. There are spherical modes that we analyze with the use of a spherically symmetric code that solves the GPP system (1) in spherical coordinates. A brief description of this code used to solve the GPP equations with initial data (2) is as follows. The evolution problem is solved in spherical coordinates in the space-time domain $r \in [0, r_{max}]$ for $t \geq 0$. For this we use a finite differences approximation of the GPP equations written in spherical coordinates as in [14, 23]. The spatial discretization uses second order accurate stencils, with second order accurate staggered regularization at the origin. For the evolution we use the method of lines with a third order accurate Runge-Kutta integrator. Considering the radius containing the 95% of the mass of the configuration $r_{95} = 3.93$ [23], we use $r_{max} > 20$ covering a domain various times bigger than such radius and use a base resolution Δr in a convergence regime.

Axial code. In order to follow the evolution of the system for non spherical perturbations, we solve the GPP system (1) with initial conditions given by (2). For this we use a code in cylindrical coordinates to solve the equations in the space-time domain $\varrho \in [0, \varrho_{max}] \times z \in [-z_{max}, z_{max}]$ for $t \geq 0$ and $\varrho_{max} = z_{max} = 20$. This

domain is sufficient to contain various times the scale r_{95} . The numerical implementation uses a finite differences method to discretize the system of equations on a 2D uniformly discrete spatial domain, with resolution in a convergent regime $\Delta\varrho = \Delta z = 0.025r_{95}$. For the time integration we again use the method of lines with a third order accurate integrator. More details about the numerical methods can be found in [24, 26].

Boundary conditions are very important since we are to analyze oscillation modes because the wave function could be reflected from the boundaries and promote the formation of certain unphysical modes. In order to avoid this, for the wave function we impose a sponge consisting of an imaginary potential, which is non-zero near the boundary according to the profile [23, 26]. For the gravitational potential, in the spherically symmetric case we impose a monopolar boundary condition, whereas in the axially symmetric code we use a multipolar expansion. The analysis presented below was double checked with evolutions carried out in a second domain twice as big as the previous one $\varrho \in [0, 2\varrho_{max}] \times z \in [-2z_{max}, 2z_{max}]$ with which we confirm our results. This fact assures that the boundary location does not affect the results shown below.

Detectors. It is very comfortable to track the behavior of the configuration by monitoring a scalar of the density, for instance its value at the coordinate origin. This is specially useful in spherically symmetric configurations and that is what we monitor in the case of spherical perturbations. In the case of non-spherical perturbations we measure the value of the density at Detector 1 located at $D_1 = (\varrho_D, 0)$ and at Detector 2 at $D_2 = (0, z_D)$ with the aim of measuring oscillation modes from different angles along the two coordinate axes. Although we use detectors at various positions along the ϱ and z axes, we did not find differences in the frequency modes found, and only present the results for the specific location with $\varrho_D = z_D = 2 \simeq r_{95}/2$.

Numerical perturbation. First we show that numerical truncation errors suffice to perturb the equilibrium configuration. This is a real perturbation with a fundamental frequency mode even though $\delta M = 0$. In order to illustrate the resulting perturbations, in the top of Figure 1 we show the central value of the density for three values of the numerical resolution $\Delta r_1 = 0.01r_{95}$, $\Delta r_2 = \Delta r_1/2$, $\Delta r_3 = \Delta r_1/2$. The amplitude of the oscillations of the central value of ρ using Δr_1 is four times the one using Δr_2 , which is four times the one using Δr_3 . This also shows the convergence of the code [14] and similar plots are found for the axi-symmetric code.

From now on we concentrate in perturbations of finite mass. We thus apply a spherical perturbation using (2) for the case $l = 0$. We evolve the initial wave function Ψ_0 with the spherically symmetric code, measure the central density and show its time-series for a given time-window at the left in Figure 1. In order to determine the dominant frequency modes we calculated the Fourier Transform (FT) of the time series of the central density and

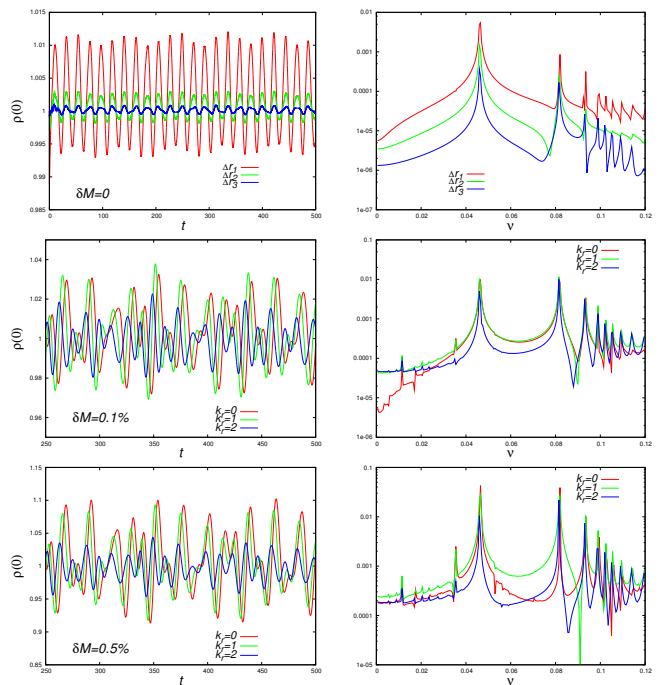


FIG. 1. Central value of the density in a given time window and its FT. At the top we show the results for the case of purely numerical perturbation with three different resolutions that show the second order convergence of the code. In the middle and bottom we present the also the central density in time and its FT for the explicit perturbations using (2) with $k_r = 0, 1, 2$ for $\delta M = 0.1\%$ and 0.5% .

show the spectrum also in Figure 1. The result is that there are two peaks indicating two dominating modes with frequencies at $\nu_1 = 0.046$ and $\nu_2 = 0.0815$.

Perturbations with $l = 1$. This case follows the prescription (2) for $l = 1$. The initial Ψ_0 is evolved using the axial code and we produce the time-series corresponding to the density measured at detectors D_1 and D_2 . Then we calculate the FT that we show in Fig. 2, for the three values of the wave number k_r , and the two mass contributions of the perturbation $\delta M = 0.1\%$, 0.5% .

The frequencies we consider associated to the configuration and not due to a particular feature of the perturbation, are those that show a peak for the three values of k_r , and the two values of δM , otherwise we consider it only a feature. Features are for instance the first peak measured by D_1 along the ϱ -axis with a frequency about $\nu \sim 0.004$, which is not a peak for $k_r = 0$ and $k_r = 2$. Another one is that measured by D_2 with frequency $\nu \sim 0.027$, because it is not a peak for any of the values of k_r and the two values of δM .

We now turn to discuss the first peaks we consider to be perturbation independent. The first important mode in the spectrum is the one found with the spherical perturbations, which is triggered by the $l = 1$ perturbation, measured by detectors D_1 and D_2 with frequency $^{10}\nu^e = ^{10}\nu^z = 0.046$. There are two other and more

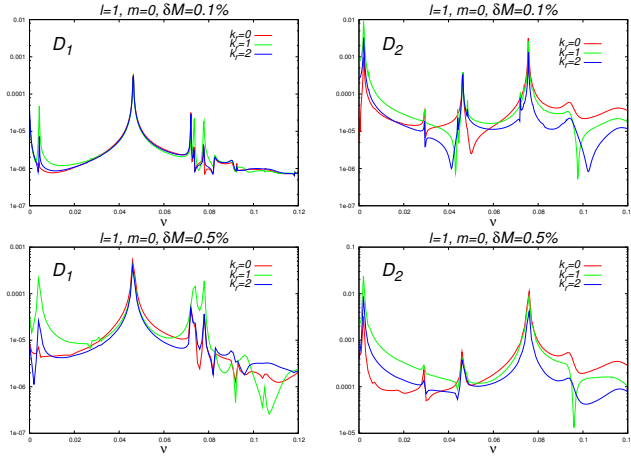


FIG. 2. Spectrum of the perturbations with $l = 1, m = 0$ mode. On the left the results measured by D_1 located at the ϱ -axis and D_2 and on the right side those measured by D_2 located at the z -axis.

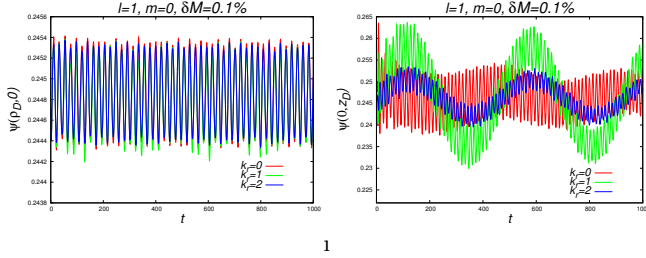


FIG. 3. Time series of the density at detector D_1 at the left and D_2 at the right. There is a low frequency mode measured clearly by D_2 .

powerful ones measured by D_2 , one of them with frequency $^{10}\nu \sim 0.076$ that is triggered only by this perturbation and a second one is a peak with very low frequency $\nu \sim 0.002$, that deserves some comments. This mode can be seen clearly from the time series of the density by detector D_2 , as shown in Fig. 3 for the perturbation with $\delta M = 0.1\%$. The period is of around 500 units of time, that corresponds to the first peak close to the axis in the right side of Fig. 2. This frequency mode is particularly interesting because it has been triggered only by $l = 1$ perturbations.

Perturbations with $l = 2$. For this we apply perturbation (2) for solely $l = 2$. Again, the density is measured at D_1 and D_2 and produce the FT of the resulting time-series, which are shown in Fig. 4. For all the wave numbers k_r , and the two values of δM there are three frequencies that are triggered, which unlike the case $l = 1$ are equally measured along the ϱ and z - axes. The first one of them is the one corresponding to the spherical mode with $^{20}\nu \sim 0.046$, a second one measured by D_1 for $l = 1$ with frequency $^{20}\nu \sim 0.072$ and a third one triggered only by this perturbation with frequency $^{20}\nu \sim 0.091$.

Spectroscopy and discussion. Collecting the informa-

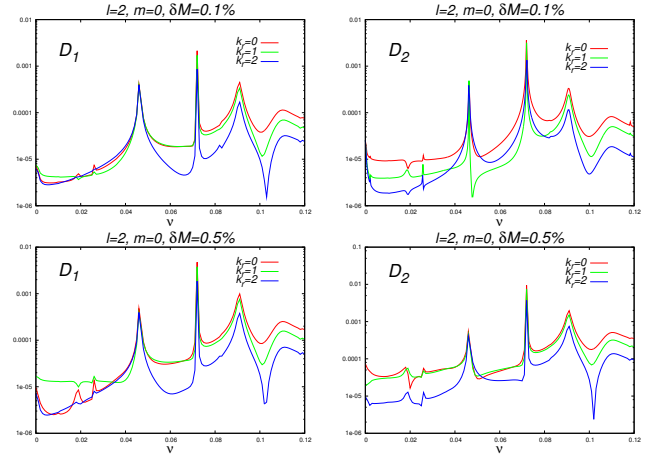


FIG. 4. Spectrum of the perturbations with the $l = 2, m = 0$ mode. On the left the results measured by detector D_1 and on the right those measured with detector D_2 .

Mode	Detector D_1	Detector D_2	T (Gyr)
$l = 0, m = 0$	$\nu_1 = 0.0460$	$\nu_1 = 0.0460$	1.65
	$\nu_2 = 0.0815$	$\nu_2 = 0.0815$	0.93
$l = 1, m = 0$	$^{10}\nu_1^{\varrho} = 0.046$	$^{10}\nu_0^z = 0.002$	37.1
	$^{10}\nu_2^{\varrho} = 0.072$	$^{10}\nu_1^z = 0.046$	1.65
		$^{10}\nu_2^z = 0.076$	1.05
	$^{10}\nu_3^{\varrho} = 0.078$		1
$l = 2, m = 0$	$^{20}\nu_1^{\varrho} = 0.046$	$^{20}\nu_1^z = 0.046$	1.65
	$^{20}\nu_2^{\varrho} = 0.072$	$^{20}\nu_2^z = 0.072$	1.05
	$^{20}\nu_3^{\varrho} = 0.091$	$^{20}\nu_3^z = 0.091$	0.84

TABLE I. Frequencies measured along the radial direction with detector D_1 and along the z -axis with detector D_2 . At the right column the period of oscillation of each mode assuming $m = 2.5 \times 10^{-22} eV$ and core radius $r_c = 1 \text{ kpc}$.

tion above, the dominant peak frequencies are summarized in Table I. The first interesting frequency is that of the radial mode which is excited by the three types of perturbation with frequency $\nu_1 = ^{10}\nu_1^{\varrho} = ^{10}\nu_2^z = ^{20}\nu_1^{\varrho} = ^{20}\nu_1^z = 0.046$. There is a second frequency produced only by the spherical perturbations $l = 0$ with frequency $\nu_2 = 0.0815$.

The third interesting mode is triggered by the axial perturbations with frequency $^{10}\nu_2^{\varrho} = ^{20}\nu_2^{\varrho} = ^{20}\nu_2^z = 0.072$. It is measured only along the radial direction when the perturbation is of type $l = 1, m = 0$ and along the two axes when applying the $l = 2, m = 0$ perturbation. Notice that perturbation $l = 2, m = 0$ excites modes that show the same frequency along the radial and axial directions, which indicates they are isotropic.

Perhaps the most interesting mode is the one triggered only by the $l = 1, m = 0$ perturbation with low frequency $^{10}\nu_0^z \sim 0.002$. This mode is measured along the z -axis. It has a frequency similar to that found in density of configurations resulting from head-on mergers [20]. The

distribution of matter in head-on mergers is consistent with the $l = 1, m = 0$ perturbation mode used here. This mode becomes important since head-on mergers result in a single blob whose density oscillates with amplitudes changing even in two orders of magnitude. A catastrophic result of this scenario is that perhaps luminous matter could not survive to such mergers as shown in [21], an effect that could serve to determine some predictions on restrict the viability of this dark matter model.

Translation to physical units. A canonical first interesting frequency to look at, is the equilibrium configuration eigenvalue $\gamma = 0.69223$, for the workhorse configuration with central wave density equals to one [23]. In fact this frequency corresponds to $\nu_e = \gamma/(2\pi) \simeq 0.11017$, located at the right side of the frequency domain in Figs. 1, 2 and 4. It is interesting that this mode is not reflected in the FTs in our figures. In order to estimate the period in physical units, one possibility is to fix the mass of the boson and the radius of the configuration as done in [15], where the period corresponding to γ or ν_e is given by

$T_e = 6.9 \times 10^8 \left(\frac{2.5 \times 10^{-22} \text{eV}}{m} \right) \left(\frac{r_c}{1 \text{kpc}} \right)^2$ yr, where r_c is the core radius the density profile of an equilibrium configuration is fitted with, and m is the boson mass. Using this formula with $r_c = 1 \text{kpc}$ and $m = 2.5 \times 10^{-22} \text{eV}$, $T_e = .69 \text{Gyr}$ and we calculate the period of the oscillations triggered by the various perturbation modes that we show in the Table. An additional exercise is to consider small structures with $r_c = 0.1 \text{kpc}$, the period of each mode will be two orders of magnitude smaller than those in the Table, which can again have an effect on luminous matter and then impose restrictions or predictions to the model.

ACKNOWLEDGMENTS

This research is supported by grants CIC-UMSNH-4.9, CONACyT 258726 and CONACyT 106466.

-
- [1] T. Matos and L. A. Ureña-López, Classical Quantum Gravity 17, L75 (2000)
 - [2] R. Hlozek, D. Grin, J. E. Marsh, P. G. Ferreira, Phys. Rev. D 91, 103512 (2015)
 - [3] L. Hui, J. P. Ostriker, S. Tremaine, and E. Witten, Phys. Rev. D 95, 043541 (2017)
 - [4] S-R. Chen, H-Y. Schive, T. Chiueh, MNRAS 468, 1338 - 1348 (2017)
 - [5] H-Y. Schive, T. Chiueh, Tzihong, T. Broadhurst, K-W. Huang, ApJ 818, 89 (2016)
 - [6] X. Du, C. Behrens, J. C. Niemeyer, B. Schwabe, Phys. Rev. D 95, 043519 (2017)
 - [7] V. H. Robles, T. Matos, ApJ 763, 19 (2013)
 - [8] T. Bernal, V. H. Robles, T. Matos, MNRAS 468, 3135 - 3149 (2017)
 - [9] H-Y. Schive, T. Chiueh, T. Broadhurst, Nature Phys. 10, 496-499 (2014)
 - [10] H-Y. Schive, M-H. Liao, T-P. Woo, S-W. Wong, T. Chiueh, T. Broadhurst, W-Y. P. Huang, Phys. Rev. Lett. 113, 261302 (2014)
 - [11] D. J. Marsh, P. G. Ferreira, Phys. Rev. D 82, 103528 (2010)
 - [12] T. Matos, A Vázquez-González, J. Magana, MNRAS, 389, 13957 (2009)
 - [13] F. S. Guzmán and L. A. Ureña-López, Phys. Rev. D 68, 024023 (2003)
 - [14] F. S. Guzmán and L. A. Ureña-López, ApJ 645, 814819 (2006)
 - [15] P. Mocz et al. MNRAS 471, 4559 - 4570 (2017)
 - [16] P-H. Chavanis, Eur. Phys. J. Plus, 132, 248 (2017)
 - [17] B. Schwabe, J. C. Niemeyer, J. F. Engels, Phys. Rev. D 94, 043513 (2016)
 - [18] P-H. Chavanis, e-print: arXiv: 1810.08948
 - [19] D. J. E. Marsh, J. C. Niemeyer, e-print: arXiv:1810.08543
 - [20] A. A. Aviléz, F. S. Guzmán, in preparation.
 - [21] F. S. Guzmán, J. A. González, and J. P. Cruz-Pérez, Phys. Rev. D 93, 103535 (2016)
 - [22] L. Pitaevskii and S. Stringari, Bose-Einstein Condensation, International Series of Monographs on Physics (Oxford University Press, New York, 2003).
 - [23] F. S. Guzmán and L. A. Ureña-López, Phys. Rev. D 69, 124033 (2004)
 - [24] A. Bernal and F. S. Guzmán, Phys. Rev. D 74, 103002 (2006)
 - [25] W. Hu, R. Barkana, and A. Gruzinov, Phys. Rev. Lett. 85, 1158 (2000).
 - [26] A. Bernal and F. S. Guzmán, Phys. Rev. D 74, 063504 (2006)